Letter

All-optical method for generating transient microstructured targets in laser ion acceleration

Ying Gao [1,2,*,†] Pengjie Wang [1,*,‡] Bin Liu [3,4,*] Shirui Xu [1] Shiyou Chen [1] Yinren Shou [1] Jianbo Liu [1] Zhusong Mei [1] Zhengxuan Cao [1] Tianqi Xu [1] Zhipeng Liu [1] Zhuo Pan [1] Defeng Kong [1] Ziyang Peng [1] Yulan Liang [1] Tan Song [1] Xun Chen [1] Qingfan Wu [1] Yujia Zhang [1] Jiarui Zhao [1] Wei Qi [5] Zhigang Deng [5] Yanying Zhao [1] Fuyuan Wu [6] Matt Zepf [4] Rafael Ramis [6] Paul R. Bolton [2] Xueqing Yan [1,7] Wenjun Ma [1,§] and Jörg Schreiber [2,‖]

[1] *State Key Lab of Nuclear Physics and Technology, School of Physics, Peking University, Beijing 100871, China*

[2] *Fakultät für Physik, Ludwig-Maximilians-Universität München, D-85748 Garching, Germany*

[3] *Guangdong Institute of Laser Plasma Accelerator Technology, Guangzhou 510080, China*

[4] *Helmholtz Institute Jena, Fröbelstieg 3, D-07743 Jena, Germany*

[5] *China Science and Technology on Plasma Physics Laboratory, Laser Fusion Research Center, China Academy of Engineering Physics, Mianyang 621900, China*

[6] *E.T.S.I. Aeronáutica y del Espacio, Universidad Politécnica de Madrid, E-28040 Madrid, Spain*

[7] *Collaborative Innovation Center of Extreme Optics, Shanxi University, Shanxi 030006, China*

(Received 10 July 2020; revised 19 March 2024; accepted 23 September 2024; published 31 October 2024)

We demonstrate an all-optical method that online produces "microstructured" targets by manipulating a Laguerre-Gaussian (LG) prepulse. Besides the enhancement of the proton number, the cutoff energy is nearly doubled. Such transient "microstructured" targets are characterized using both offline and online approaches. Based on probe experiments and hydrodynamic simulations, we develop a simple model to describe the electron density distribution upon the arrival of the main pulse. Two-dimensional particle-in-cell simulations reveal that the annular plasma acts as an oscillating cavity for hot electrons and results in a cascaded acceleration effect. The combination of low-intensity LG prepulses and ultraintense Gaussian pulses opens another avenue for fine-tuning laser-plasma interactions spatiotemporally in interdisciplinary applications.

DOI: 10.1103/PhysRevResearch.6.L042031

The intense laser-plasma interaction has been a broad and evolving research field over the last decades. When intense laser pulses irradiate targets, several kinds of radiation, including high-energy electrons, ions, x rays, or gamma rays, can be generated. Such particles and photons with unique characteristics have broad applications both in fundamental science and society, such as fast ignition [1], radiography [2], cancer therapy [3], and the generation of warm dense matter [4]. Apart from intense lasers, targets have been playing a key role in laser-plasma interactions.

Laser irradiation experiments using microstructured targets [5] offer an excellent and versatile platform for studying electron and ion acceleration [6,7], fusion [8], and high-energy-density physics. For example, varying wire/channel targets demonstrate higher laser absorption efficiency [9] and have shown superior performance in microscale fusion [8] and ion acceleration [10,11]. When the target channels have a diameter comparable to the laser focal spot size, the guidance of laser propagation [12] inside the channel becomes dominant, and cone targets have similar effects [13]. Additionally, modified structures along the target surface, such as "grating" targets, have been developed. It has been reported that these structures can generate relativistic surface plasmons, enhancing the energy and number of emitted electrons [14]. Moreover, laser irradiation of microstructured targets has demonstrated the generation of quasimonoenergetic proton beams [7]. Especially, when solid foils with limited transverse extent are used, electrons reflected from the target edges [15] can maintain a hotter, denser electron sheath at the rear side of the targets for an extended period resulting in an enhanced ion acceleration.

However, those targets employed in experiments are routinely fabricated by complex procedures, which makes it challenging to perform at a high repetition rate. On the one hand, much effort needs to be devoted to target fabrication to obtain a sufficient number of shots for applications. On the other hand, the precise alignment of high-power laser pulses with microstructured targets remains a long-term challenge, affecting the performance and reducing the stability.

In this Letter, we demonstrate an all-optical method to produce microstructured targets on a nanosecond timescale before high-power laser pulses. By introducing a Laguerre-Gaussian (LG) prepulse before the main pulse, an annular

*These authors contributed equally to this work.
† Contact author: ying_gao@pku.edu.cn
‡Present address: Institute of Radiation Physics, Helmholtz-Zentrum Dresden-Rossendorf, Dresden, Germany.
§Contact author: wenjun.ma@pku.edu.cn
‖Contact author: joerg.schreiber@lmu.de

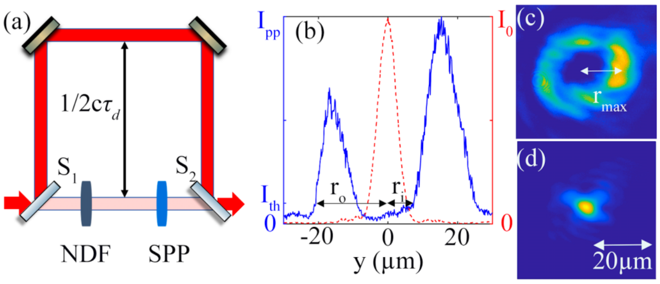

FIG. 1. (a) Schematic of the experimental setup. S_1, S_2: beam splitter, combiner ($T/R = 1/9$). $\tau_d = 1.7$ ns. (b) The intensity profiles of the LG prepulse (blue) and the main pulse (dashed red). r_i and r_o are determined by the damage threshold intensity $I_{\rm th}$ and the peak intensity $I_{\rm pp}$. The focal image of (c) the LG prepulse and (d) the main pulse.

preplasma can be generated when interacting with flat foil targets. The central undisturbed foil target is tailored into an isolated plate with a lateral size of several to tens of micrometers. Experimental results showed a significant enhancement of proton cutoff energy and number. We developed a simple model to describe the preplasma density distribution, and two-dimensional particle-in-cell (2D PIC) simulations revealed that the annular preplasma surrounding the isolated plate acted as an oscillating cavity for hot electrons, resulting in the cascaded acceleration of protons as they bounced off the cavity's outer edge.

We introduced the LG prepulse in the chirped pulse amplification chain before the final amplification stage of the Ti:sapphire laser system, a compact laser plasma accelerator (CLAPA), as depicted in Fig. 1(a). The beam splitter (S_1) transmitted 10% of the pulse energy while the remaining 90% was reflected and directed to the beam combiner (S_2). The two pulses, with a fixed time delay of 1.7 ns, were then recollimated. The LG prepulse was generated by inserting a 20-mm-diameter, 1-mm-thick silica, 64-stair-step spiral phase plate (SPP) in the prepulse arm. The SPP, when transmitting, imprints a helical variation of phase, creating an annular-shaped far-field transverse intensity distribution of the prepulse that resembles an LG mode with an azimuthal index of $m = 6$. The spatial laser intensity distribution on the target, located at $z = 0$, can be described in cylindrical coordinates [16] as follows,

$$I_p^m(r) \propto (\sqrt{2}r/\omega_0)^{2m}\left[L_p^m\left(2r^2/\omega_0^2\right)\right]^2 e^{(-2m^2/\omega_0^2)}, \qquad (1)$$

where r is the radial distance, L_p^m is the Laguerre polynomial, and ω_0 is the beam waist. The radius of maximum intensity $r_{\rm max} = \omega_0\sqrt{m/2}$ for $p = 0$.

The collimated LG prepulse and the main pulse were expanded, amplified, and compressed in sequence. The far-field intensity distribution of each pulse was individually measured and shown in Figs. 1(c) and 1(d). The main pulse had an energy of approximately 1 J, a full width at half maximum (FWHM) diameter of 6 μm, and a pulse duration of 30 fs, resulting in a peak intensity of 8×10^{19} W/cm^2. Figure 1(c) displays the LG prepulse's far field, with a peak intensity of 1.6×10^{18} W/cm^2 at $r_{\rm max} = 15$ μm, achieved without neutral density filters (NDFs).

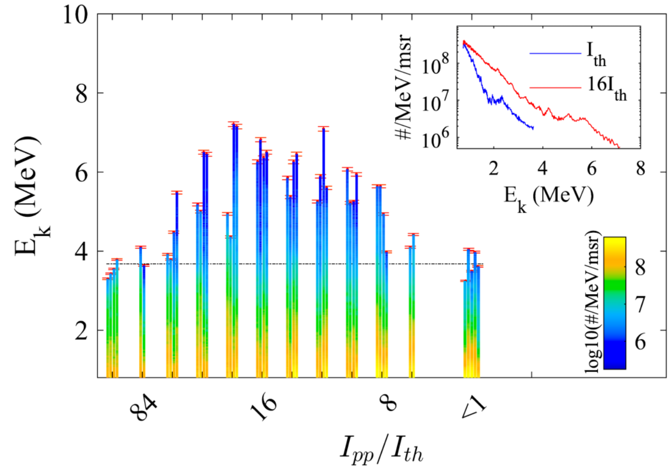

FIG. 2. Experimental proton spectra as a function of $I_{\rm pp}$. The black line represents the average maximum energy with $I_{\rm pp} < I_{\rm th}$. Inset: The two curves correspond to $16I_{\rm th}$ (red) and $I_{\rm th}$ (blue) cases, and r_i and r_o for each case are 3 and 25 μm for $16I_{\rm th}$ and 15 and 15 μm for $I_{\rm th}$, respectively.

First, we conducted the proton acceleration experiments driven solely by the main pulse using plastic targets with a thickness of 2 μm, which provided a benchmark. To measure the proton spectra, we employed a Thomson parabola spectrometer that featured a 0.3-T, 48.5-mm-long magnetic field, and an electric field with a strength of 7000 V/mm over a distance of 250 mm. This allowed us to disperse the ion beams based on their kinetic energy and charge-to-mass ratios [17]. Downstream of the spectrometer, a microchannel plate and a phosphor screen are used to display the ion signal, which is recorded by an electron-multiplying charge-coupled device. The average cutoff energy for protons is 3.8 MeV, as indicated by the black line in Fig. 2.

Subsequently, we irradiated targets using only the LG prepulse, gradually reducing the intensity. Once the peak intensity $I_{\rm pp}$ exceeded the threshold ($I_{\rm th} \sim 2.4 \times 10^{13}$ W/cm^2) of plastic targets [18], a hole resembling the outermost contour of the ionization threshold intensity appeared on the target. When $I_{\rm pp}$ in the ring was below the threshold value, no damage occurred. This suggests that the ionized region is highly localized, and the radius of the undisturbed central region, referred to as $r_i(I_{\rm pp})$, can be adjusted by varying the intensity of the LG prepulse. The outer boundary of the plasma is denoted by $r_o(I_{\rm pp})$. Note that the LG mode generated in experiments did not have perfect spatial contrast [19,20]. As a result, when $I_{\rm pp}$ exceeded $30I_{\rm th}$, the intensity in the center of the LG focal spot would inevitably surpass the plasma formation threshold. This can trigger plasma formation and may even destroy the whole central region.

Figure 2(a) displays the logarithmically color-coded differential proton spectra plotted against kinetic energy along the vertical axis. The intensity of the LG prepulse was varied by modulating its energy while keeping the energy of the main pulse constant. This variation is represented on the horizontal x axis. We can see that the LG prepulse has no significant influence on the proton spectra when $I_{\rm pp} < I_{\rm th}$. Then, the increase of $I_{\rm pp}$ results in an enhancement both in the proton number and the cutoff energy. Proton

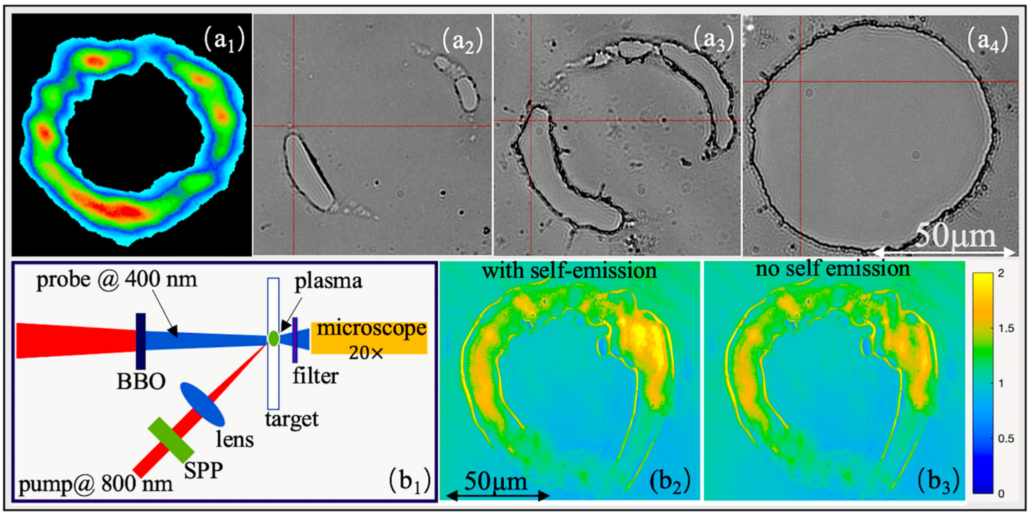

FIG. 3. Focusing pattern of LG prepulse (a_1) and the residual target images obtained by shooting plastic targets with $I_{\rm th}$ (a_2), $4I_{\rm th}$ (a_3), and $8I_{\rm th}$ (a_4), respectively. Experimental LG pump-probe setup (b_1); the processed images: (pump+probe)/background (b_2); (pump+probe-self-emission)/background (b_3); the probe pulse is 1.7 ns after the irradiation with the LG pulse (pump) with a peak intensity 2×10^{14} W/cm^2.

emission becomes stronger and the emitted protons are most energetic when $I_{\rm pp}$ is approximately between $8I_{\rm th}$ and $20I_{\rm th}$. However, when $I_{\rm pp} > 30I_{\rm th}$, the energy and number of protons decrease significantly, with the number falling below the case without the LG prepulse. In this case, the nonzero intensity at the center of the ring meets the condition for preplasma generation, leading to r_i ($I_{\rm pp} > 30I_{\rm th}$) becoming zero. Additionally, the reduced plasma density gradient at the target rear surface, generated by this LG prepulse, can also reduce the performance of proton acceleration [21]. The inset in Fig. 2 features two representative energy spectra of protons ($I_{\rm th}$ and $16I_{\rm th}$) measured in experiments.

It is worth noting that using the cross-polarization wave (XPW) generation front-end makes the nanosecond pedestal lower than 10^{10} W/cm^2 and the picosecond pedestal before -20 ps lower than 10^{11} W/cm^2 [22], which are both lower than the target's damage threshold [18]. Hydrodynamic simulation and analysis indicate that the scale length of the preplasma caused by the rising edge of the main pulse (∼1 μm) is much smaller than that of the preplasma produced by the LG prepulse (∼10 μm). So we can conclude that neither the nanosecond nor the picosecond prepulses of the main laser significantly influence our scheme.

To demonstrate the target structure imprinted by the intensity distribution of the LG prepulse, an LG focal ring with a similar peak intensity was employed, as shown in Fig. 3(a_1). When $I_{\rm pp} = I_{\rm th}$, only several dots appeared on the flat foil target [Fig. 3(a_2)]. Increasing $I_{\rm pp}$ to $4I_{\rm th}$, two thin bands [Fig. 3(a_3)] with a width comparable to that of the LG prepulse can be identified, which also indicated a trend that using a higher intensity, an enclosed circular target could be cut from the flat foil target. In Fig. 3(a_4), a large hole was observed in the case of $I_{\rm pp} = 8I_{\rm th}$, and its diameter was similar to the outer contour of the target damage threshold intensity of the LG prepulse. It was inferred that an isolated plate was generated and completely detached from the flat foil target. The diameter of the central microtarget can be adjusted by the intensity distribution of the LG prepulse and its azimuthal index. For example, as the intensity $I_{\rm pp}$ increases, r_i is expected to decrease while r_o will increase, as illustrated in Fig. 1(b).

A pump-probe experiment was performed to confirm the generation of transient micro-structured targets. In Fig. 3(b_1), a beta barium borate (BBO) crystal is employed to perform frequency doubling of a femtosecond pulse as the probe beam. The other 800-nm central wavelength fs pulse is converted into an LG mode via an SPP and subsequently focused onto the target using a lens. The intensity of the LG pulse is adjustable and the probe beam's time delay precision is 0.1 ns, determined by the oscilloscope's sampling frequency. A 20× microscope system is situated in the probe beam path, and a bandpass filter (350–550 nm) is inserted to filter out the fundamental wave and partial plasma self-emission. This enables capturing a snapshot of the 400-nm probe beam as it passes through the annular plasma. In this study, we are interested in the extent of the small central target region and the surrounding plasma's density distribution after a longer period (ns) of LG prepulse acting on the target. Under this scenario, where the plasma density has approached or dropped below the critical density, the probe beam can penetrate through with a higher transmission ratio compared to the background image obtained with a probe beam illuminating a plastic target, as shown in Fig. 3(b_2). The center on the plasma ring, where it is thickest, appears brightest. Figure 3(b_3) confirms that disturbances due to plasma self-emission or scattering of the pump pulse are negligible. Therefore, we have a probe snapshot of the annular, transient plasma.

Based on the pump-probe experiment and discussion above, it seems that the plasma has not significantly expanded transversely until the arrival of the main pulse. We conducted two-dimensional hydrodynamic simulations utilizing the MULTI-2D code [23,24] to obtain the longitudinal expansion state [25]. Then, we employed the 2D PIC simulations [25] using the plasma simulation code (PSC) [26].

The proton spectra extracted from the PIC simulation 1.3 ps after the main pulse interaction are shown in Fig. 4(h).

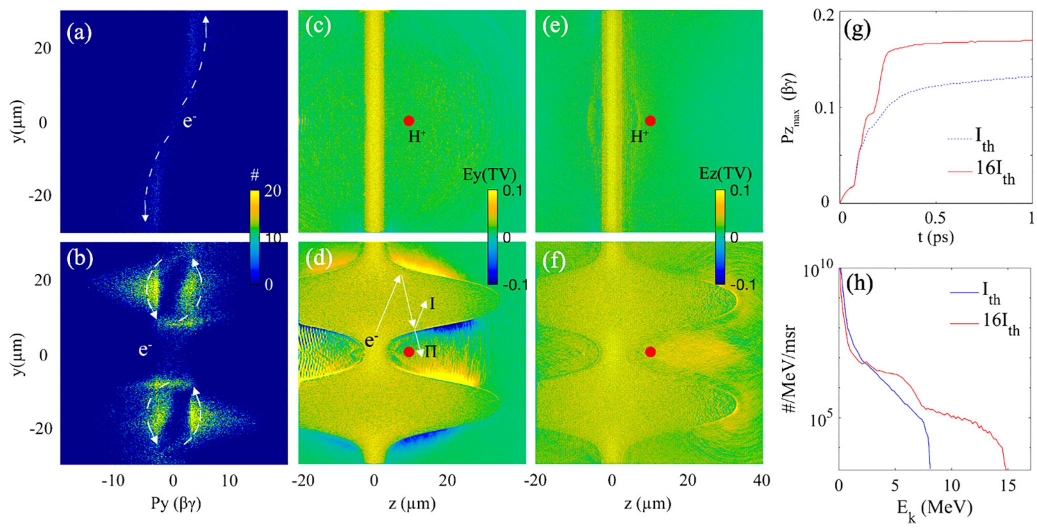

FIG. 4. Results obtained from PIC simulations. (a), (b) Transverse phase space of electrons with energies 0.5–5 MeV at $t = 0.15$ ps and trajectories. (c), (d) Transverse field distribution at $t = 0.15$ ps. (e), (f) Acceleration field distribution at 0.2 ps. (g) The evolution of momentum $Pz_{\max}$ of the most energetic protons [depicted as red dots in (c)–(f)]. Plots in (a), (c), (e) and (b), (d), (f) correspond to I_{th} and $16I_{\text{th}}$ cases, respectively. (h) The proton spectra at 1.3 ps after the main pulse interaction for two cases.

The values of r_i and r_o are extracted from the intensity contour and n_{ring} is adjusted to n_0 and $0.05n_0$ for the respective cases. Similar to the experimental results, increasing I_{pp} from I_{th} (blue) to $16I_{\text{th}}$ (red) leads to an enhancement of proton acceleration. However, for higher values of I_{pp}, e.g., $84I_{\text{th}}$, proton acceleration becomes inefficient due to the generation of preplasma in the center caused by the low spatial contrast of the imperfect LG mode.

To understand the reason for the energy enhancement, we have considered the two representative cases I_{th} and $16I_{\text{th}}$. We plot the temporal evolution of $Pz_{\max}$ for the two cases in Fig. 4(g). The slope $dPz_{\max}/dt$ is proportional to the acceleration field E_z and it is indistinguishable for both cases until $t = 0.1$ ps. For case I_{th}, the acceleration field significantly decreases after about 0.2 ps (blue). However, with annular plasma present (case $16I_{\text{th}}$), the momentum is boosted further, in particular between 0.18 and 0.25 ps (red). The fastest protons hence have been accelerated by a second strong longitudinal field.

Figures 4(e) and 4(f) illustrate snapshots of the longitudinal electric field E_z in scenarios without and with annular plasma, respectively. The position of the fastest protons is marked by a red dot. At 0.2 ps, a second acceleration field emerges just behind the initial acceleration zone in the case of annular plasma. This field is generated by thermal electrons that are bounced from the outer edge of the annular plasma region, as evidenced by the phase-space distribution of electrons in Fig. 4(b). The transverse electric field E_y [Fig. 4(d)] plays a vital role in confining these thermal electrons in the annular plasma region for an extended time. It takes approximately 0.2 ps for thermal electrons with MeV-level kinetic energies to be bounced back in the transverse direction, covering a travel distance of about 50 μm. Consequently, the second stage acceleration comes into effect once the first stage acceleration has ended, resulting in the observed cascaded acceleration shown in Fig. 4(g). In contrast, without such microstructured plasma, thermal electrons spread directly from the center to the periphery region [Fig. 4(a)].

To verify the wide applicability of the effect of this microstructured target on proton acceleration, we extended the laser parameters numerically to petawatt (PW) fs lasers with a pulse duration of 30 fs and a FWHM of 5.4 μm, corresponding to a laser intensity of 5×10^{20} W/cm^2. Through 2D PIC simulations, we compared three different examples: a large flat target (thickness 100 nm, same below), a completely isolated 6-μm small target, and a barrel-shaped plasma with uniform density surrounding a 6-μm small target. We found that the proton cutoff energy for the large flat target was 45 MeV, for the isolated small target it was 77 MeV, and for the third scenario with the barrel-shaped plasma it was 110 MeV. Therefore, we conclude that this cascaded acceleration mechanism can be extended to higher-power PW laser cases. For the PW laser, we found that even without a preplasma in front of the central small target, some of the electrons in the barrel-shaped plasma would be pulled towards the center, thus focusing the main laser pulse. This will be discussed in a future publication.

In summary, we have demonstrated that an isolated microfoil target surrounded by an annular plasma can be produced by an LG prepulse before the arrival of the main laser pulse, and such a transient microstructured target generated by the all-optical method can significantly enhance proton acceleration. In future studies, one can widen the diameter and width of the annular plasma cavity to match the timing of the fastest proton and the second stage acceleration field E_z perfectly, which can be extended to higher laser intensity experiments. This has been confirmed by simulations.

It is important to note that our experimental method has a certain applicability scope. For the main laser, which operates at PW levels, the intensity of the nanosecond prepulse must remain below the target's damage threshold. Given a peak intensity of 10^{21} W/cm^2, the nanosecond prepulse intensity should be below 10^{11} W/cm^2, meaning that the nanosecond contrast should be better than 10^{-10}. Besides the XPW or optical parametric chirped-pulse amplification front-end, a plasma mirror system [27] is proposed to enhance the contrast ratio of the main laser. After that, a small aperture prepulse can be extracted from the main pulse and converted into the LG mode to generate microstructured targets.

It would also be interesting to allow the annular plasma to expand for a longer time, which is expected to change the cavity effect into an isolation effect, as resembled by the mass-limited-target case [15]. The approach provides another idea for enhancing laser-driven ion acceleration, and more importantly, it is compatible with high-repetition-rate experiments. Our analysis suggests that the increase in performance can be attributed to a temporary oscillation cavity effect exhibited by hot electrons. This electron cavity, achieved through microplasma structuring, is an exemplary instance of "plasma electronics"—a distinct classification from "plasma photonics" (where plasma acts on photons, such as the plasma mirror [28] or the so far neglected effect of the plasma pinching) and "plasma ionics" (where plasma influences ions [29], including the Gabor lens [30]). By considering combinations of these three concepts, we can explore different methods for manipulating the parameter space of available laser-driven ion bunches at their source.

We acknowledge the support of the DFG-funded cluster of excellence Munich-Centre for Advanced Photonics, the support of National Grand Instrument Project (SQ2019YFF010006), National Natural Science Foundation of China (11775010, 61631001) and NSFC innovation group project (11921006), the support of Spanish MCIU Project No. RTI2008-098801-B-I00, and Euratom Project No. AWP17-ENR-IFE-CEA-01. P.W. acknowledges the support from Helmholtz-OCPC Postdoc Program (ZD2022020). B.L. acknowledges the support of the Guangdong High-Level Innovation Research Institute Project, Grant No. 2021B0909050006.

[1] M. Tabak, J. Hammer, M. E. Glinsky, and W. L. Kruer, Ignition and high gain with ultrapowerful lasers, Phys. Plasmas **1**, 1626 (1994).

[2] S. Corde, K. Ta Phuoc, G. Lambert, R. Fitour, V. Malka, A. Rousse, A. Beck, and E. Lefebvre, Femtosecond x rays from laser-plasma accelerators, Rev. Mod. Phys. **85**, 1 (2013).

[3] K. W. D. Ledingham, P. R. Bolton, N. Shikazono, and C. M. C. Ma, Towards laser driven hadron cancer radiotherapy: A review of progress, Appl. Sci. **4**, 402 (2014).

[4] B. Mahieu, N. Jourdain, K. Ta Phuoc, F. Dorchies, J. P. Goddet, A. Lifschitz, P. Renaudin, and L. Lecherbourg, Probing warm dense matter using femtosecond x-ray absorption spectroscopy with a laser-produced betatron source, Nat. Commun. **9**, 3276 (2018).

[5] T. Ebert, R. Heber, T. Abel, J. Bieker, G. Schaumann, and M. Roth, Targets with cone-shaped microstructures from various materials for enhanced high-intensity laser-matter interaction, High Power Laser Sci. Eng. **9**, e24 (2021).

[6] J. Snyder, L. L. Ji, K. M. George, C. Willis, G. E. Cochran, R. L. Daskalova, A. Handler, T. Rubin, P. L. Poole, D. Nasir, A. Zingale, E. Chowdhury, B. F. Shen, and D. W. Schumacher, Relativistic laser-driven electron accelerator using micro-channel plasma targets, Phys. Plasmas **26**, 033110 (2019).

[7] H. Schwoerer, S. Pfotenhauer, O. Jaeckel, K. U. Amthor, B. Liesfeld, W. Ziegler, R. Sauerbrey, K. W. Ledingham, and T. Esirkepov, Laser-plasma acceleration of quasi-monoenergetic protons from microstructured targets, Nature (London) **439**, 445 (2006).

[8] A. Curtis, C. Calvi, J. Tinsley, R. Hollinger, V. Kaymak, A. Pukhov, S. Wang, A. Rockwood, Y. Wang, V. N. Shlyaptsev, and J. J. Rocca, Micro-scale fusion in dense relativistic nanowire array plasmas, Nat. Commun. **9**, 1077 (2018).

[9] J. Park, R. Tommasini, R. Shepherd, R. A. London, C. Bargsten, R. Hollinger, M. G. Capeluto, V. N. Shlyaptsev, M. P. Hill, V. Kaymak, C. Baumann, A. Pukhov, D. Cloyne, R. Costa, J. Hunter, S. Maricle, J. Moody, and J. J. Rocca, Absolute laser energy absorption measurement of relativistic 0.7 ps laser pulses in nanowire arrays, Phys. Plasmas **28**, 023302 (2021).

[10] M. Bailly-Grandvaux, D. Kawahito, C. McGuffey, J. Strehlow, B. Edghill, M. S. Wei, N. Alexander, A. Haid, C. Brabetz, V. Bagnoud, R. Hollinger, M. G. Capeluto, J. J. Rocca, and F. N. Beg, Ion acceleration from microstructured targets irradiated by high-intensity picosecond laser pulses, Phys. Rev. E **102**, 021201(R) (2020).

[11] L. A. Gizzi, G. Cristoforetti, F. Baffigi, F. Brandi, G. D'Arrigo, A. Fazzi, L. Fulgentini, D. Giove, P. Koester, L. Labate, G. Maero, D. Palla, M. Romé, M. Russo, D. Terzani, and P. Tomassini, Intense proton acceleration in ultrarelativistic interaction with nanochannels, Phys. Rev. Res. **2**, 033451 (2020).

[12] D. B. Zou, D. Y. Yu, M. Y. Yu, T. W. Huang, A. Pukhov, H. B. Zhuo, C. T. Zhou, and S. C. Ruan, Efficient generation of $\sim$100 MeV ions from ultrashort $\sim 10^{21}$ W cm^{-2} laser pulse interaction with a waveguide target, Nucl. Fusion **59**, 066034 (2019).

[13] X. M. Li, Y. Chao, R. Xie, and D. J. Liu, Enhancement of magnetic vortex acceleration by laser interaction with near-critical density plasma inside a Hollow conical target, Laser Part. Beams **2022**, e24 (2022).

[14] L. Fedeli, A. Sgattoni, G. Cantono, D. Garzella, F. Réau, I. Prencipe, M. Passoni, M. Raynaud, M. Květoň, J. Proska, A. Macchi, and T. Ceccotti, Electron acceleration by relativistic surface plasmons in laser-grating interaction, Phys. Rev. Lett. **116**, 015001 (2016).

[15] S. Buffechoux, J. Psikal, M. Nakatsutsumi, L. Romagnani, A. Andreev, K. Zeil, M. Amin, P. Antici, T. Burris-Mog, A. Compant-La-Fontaine, E. d'Humières, S. Fourmaux, S. Gaillard, F. Gobet, F. Hannachi, S. Kraft, A. Mancic, C. Plaisir, G. Sarri, M. Tarisien, T. Toncian, U. Schramm, M. Tampo, P. Audebert, O. Willi, T. E. Cowan, H. Pépin, V. Tikhonchuk,

M. Borghesi, and J. Fuchs, Hot electrons transverse refluxing in ultraintense laser-solid interactions, Phys. Rev. Lett. **105**, 015005 (2010).

[16] G. Ruffato, M. Massari, and F. Romanato, Generation of high-order Laguerre Gaussian modes by means of spiral phase plates, Opt. Lett. **39**, 5094 (2014).

[17] T. W. Jeong, P. K. Singh, C. Scullion, H. Ahmed, K. F. Kakolee, P. Hadjisolomou, A. Alejo, S. Kar, M. Borghesi, and S. Ter-Avetisyan, Experimental evaluation of the response of micro-channel plate detector to ions with 10s of MeV energies, Rev. Sci. Instrum. **87**, 083301 (2016).

[18] D. Wang, Y. Shou, P. Wang, J. Liu, Z. Mei, Z. Cao, J. Zhang, P. Yang, G. Feng, S. Chen, Y. Zhao, J. Schreiber, and W. Ma, Laser-induced damage thresholds of ultrathin targets and their constraint on laser contrast in laser-driven ion acceleration experiments, High Power Laser Sci. Eng. **8**, e41 (2020).

[19] C. Brabetz, S. Busold, T. Cowan, O. Deppert, D. Jahn, O. Kester, M. Roth, D. Schumacher, and V. Bagnoud, Laser-driven ion acceleration with hollow laser beams, Phys. Plasmas **22**, 013105 (2015).

[20] W. P. Wang, C. Jiang, H. Dong, X. M. Lu, J. F. Li, R. J. Xu, Y. J. Sun, L. H. Yu, Z. Guo, X. Y. Liang, Y. X. Leng, R. X. Li, and Z. Z. Xu, Hollow plasma acceleration driven by a relativistic reflected hollow laser, Phys. Rev. Lett. **125**, 034801 (2020).

[21] M. Kaluza, J. Schreiber, M. I. K. Santala, G. D. Tsakiris, K. Eidmann, J. Meyer-ter Vehn, and K. J. Witte, Influence of the laser prepulse on proton acceleration in thin-foil experiments, Phys. Rev. Lett. **93**, 045003 (2004).

[22] Y. X. Geng, Q. Liao, Y. R. Shou, J. G. Zhu, X. H. Xu, M. J. Wu, P. J. Wang, D. Y. Li, T. Yang, R. H. Hu, D. H. Wang, Y. Y. Zhao, W. J. Ma, H. Y. Lu, Z. X. Yuan, C. L. Lin, and X. Q. Yan, Generating proton beams exceeding 10 MeV using high contrast 60TW laser, Chin. Phys. Lett. **35**, 092901 (2018).

[23] R. Ramis, J. Meyer ter Vehn, and J. Ramírez, MULTI2D – a computer code for two-dimensional radiation hydrodynamics, Comput. Phys. Commun. **180**, 977 (2009).

[24] F. Wu, Y. Chu, R. Ramis, Z. Li, Y. Ma, J. Yang, Z. Wang, F. Ye, Z. Huang, J. Qi, L. Zhou, C. Liang, S. Chen, Z. Ge, X. Yang, and S. Wang, Numerical studies on the radiation uniformity of Z-pinch dynamic hohlraum, Matter Radiat. Extremes **3**, 248 (2018).

[25] See Supplemental Material at http://link.aps.org/supplemental/10.1103/PhysRevResearch.6.L042031 for a discussion of the MULTI2D simulations and the details of 2D PIC simulations.

[26] H. Ruhl, *Classical Particle Simulations with the PSC Code* (Rinton, Paramus, New Jersey, 2006).

[27] I. W. Choi, C. H. Jeon, S. G. Lee, S. Y. Kim, T. Y. Kim, I. J. Kim, H. W. Lee, J. W. Yoon, J. H. Sung, S. K. Lee, and C. H. Nam, Highly efficient double plasma mirror producing ultrahigh-contrast multi-petawatt laser pulses, Opt. Lett. **45**, 6342 (2020).

[28] C. Thaury, H. George, F. Quéré, R. Loch, J.-P. Geindre, P. Monot, and Ph. Martin, Coherent dynamics of plasma mirrors, Nat. Phys. **4**, 631 (2008).

[29] W. P. Wang, H. Dong, Z. Y. Shi, Y. X. Leng, R. X. Li, and Z. Z. Xu, Collimated particle acceleration by vortex laser-induced self-structured “plasma lens”, Appl. Phys. Lett. **121**, 214102 (2022).

[30] J. A. Palkovic, F. E. Mills, C. Schmidt, and D. E. Young, Gabor lens focusing of a proton beam, Rev. Sci. Instrum. **61**, 550 (1990).